DOI: 10.34119/bjhrv8n3-290

In vitro identification of dapaconazole metabolites and enzymatic phenotyping using human liver microsomes and selective CYP450 inhibitory monoclonal antibodies

Identificação *in vitro* dos metabólitos do dapaconazol e fenotipagem enzimática utilizando microssomos hepáticos humanos e anticorpos monoclonais inibidores seletivos do CYP450

Identificación *in vitro* de metabolitos de dapaconazol y fenotipado enzimático mediante microsomas hepáticos humanos y anticuerpos monoclonales inhibidores selectivos de CYP450

DOI:10.34119/bjhrv8n3-290

Submitted: May 23th, 2025
Approved: Jun 13th, 2025

Giulia Minuti
Master's student in Pharmacology
Instituição: Departamento de Farmacologia, Faculdade de Ciências Médicas, Universidade Estadual de Campinas (UNICAMP)
Endereço: Campinas, São Paulo, Brazil
E-mail: giu.minuti@gmail.com

Alexandre Barcia Godoi
Master's in Pharmacology and Toxicology
Instituição: Departamento de Farmacologia, Faculdade de Ciências Médicas, Universidade Estadual de Campinas (UNICAMP)
Endereço: Campinas, São Paulo, Brazil
E-mail: a165201@dac.unicamp.br

Debora Bressanim de Aquino Calemi
Master's student in Pharmacology
Instituição: Departamento de Farmacologia, Faculdade de Ciências Médicas, Universidade Estadual de Campinas (UNICAMP)
Endereço: Campinas, São Paulo, Brazil
E-mail: d234945@dac.unicamp.br

Gilberto de Nucci
PhD in Pharmacology
Instituição: Departamento de Farmacologia, Faculdade de Ciências Médicas, Universidade Estadual de Campinas (UNICAMP)
Endereço: Campinas, São Paulo, Brazil
E-mail: denucci@gilbertodenucci.com

Jose Luiz da Costa
PhD in Toxicology
Instituição: Departamento de Farmacologia, Faculdade de Ciências Médicas, Universidade Estadual de Campinas (UNICAMP), Centro de Informação e Assistência Toxicológica de Campinas, Faculdade de Ciências Médicas, Universidade Estadual de Campinas (UNICAMP)
Endereço: Campinas, São Paulo, Brazil
E-mail: josejlc@unicamp.br

Natalícia de Jesus Antunes
PhD in Toxicology
Instituição: Faculdade de Ciências Médicas, Universidade Estadual de Campinas (UNICAMP)
Endereço: Campinas, São Paulo, Brazil
E-mail: nataliciaja@gmail.com

ABSTRACT
Superficial fungal infections have significantly increased in recent decades, becoming one of the most prevalent forms of infection. Fungal resistance to azole compounds has been an important focus of research in recent years. Dapaconazole, a new antifungal imidazole, was developed through radical innovation and has shown efficacy against pathogenic fungi. The objective of this study was to elucidate the main metabolites generated by phase I and phase II metabolism of dapaconazole *in vitro,* using human (HLM) and rat (RLM) liver microsomes and *in silico* tools (Meteor Nexus and GastroPlus® softwares). The isoenzymes involved in the process were also investigated by enzyme phenotyping with inhibitory antibodies against CYP450 isoenzymes. The metabolite identification was performed using liquid chromatography quadrupole time-of-flight mass spectrometry (LC-QTOF-MS). For enzyme phenotyping, a liquid chromatography quadrupole mass spectrometry (LC-MS/MS) method was employed. A total of seven metabolites were found in HLM and RLM, which five ($C_{20}H_{18}Cl_2F_3N_2O$, $C_{19}H_{16}Cl_2F_3N_2O_2$, $C_{11}H_{11}Cl_2N_2O$, $C_{19}H_{16}Cl_2F_3N_2O_2$, $C_{19}H_{14}Cl_2F_3N_2O_2$) were produced by phase I reactions, metabolized by various isoenzymes of the CYP450 (CYP1A1, CYP1A2, CYP2B6, CYP2C8, CYP2C19, CYP2D6, CYP2E1, CYP3A4), one by phase I + II ($C_{25}H_{24}Cl_2F_3N_2O_8$), and one directly by phase II ($C_{25}H_{24}Cl_2F_3N_2O_7$). *In silico* simulation models were relevant for metabolite identification and proved to be an important complement to *in vitro* experiments. The essays allowed not only determination, but also the metabolites formation rate. Differences in metabolic formation rates between species were observed, mainly for the conjugated metabolites.

Keywords: dapaconazole, imidazole, *in vitro* metabolism, microsome, enzymatic phenotyping, inhibitory antibodies, *in silico* prediction.

RESUMO
As infecções fúngicas superficiais têm aumentado significativamente nas últimas décadas, tornando-se uma das formas mais prevalentes de infecção. A resistência dos fungos aos compostos azólicos tem sido um foco importante de pesquisa nos últimos anos. O dapaconazol, um novo antifúngico imidazólico, foi desenvolvido por meio de inovação radical para atuar contra fungos patogênicos. O objetivo deste estudo foi elucidar os principais metabólitos do dapaconazol gerados por metabolismo de fase I e II *in vitro*, utilizando microssomos hepáticos humanos (HLM) e de ratos (RLM), além de ferramentas *in silico* para predição (*softwares* Meteor Nexus e GastroPlus®). Foram determinadas também as isoenzimas envolvidas no processo por meio de fenotipagem enzimática com anticorpos inibidores contra as isoenzimas

do CYP450. A identificação dos metabólitos foi realizada utilizando cromatografia líquida acoplada a espectrometria de massa quadrupolo tempo de voo (LC-QTOF-MS). Para a fenotipagem enzimática, um método de cromatografia líquida acoplada a espectrometria de massas sequencial (LC-MS/MS) foi empregado. Ao todo, sete metabólitos foram identificados em HLM e RLM, sendo que cinco foram formados por reações de fase I ($C_{20}H_{18}Cl_2F_3N_2O$, $C_{19}H_{16}Cl_2F_3N_2O_2$, $C_{11}H_{11}Cl_2N_2O$, $C_{19}H_{16}Cl_2F_3N_2O_2$, $C_{19}H_{14}Cl_2F_3N_2O_2$), mediadas por diversas isoenzimas do CYP450 (CYP1A1, CYP1A2, CYP2B6, CYP2C8, CYP2C19, CYP2D6, CYP2E1, CYP3A4), um metabólito foi gerado por reações combinadas de fase I e II ($C_{25}H_{24}Cl_2F_3N_2O_8$), e um outro exclusivamente por fase II ($C_{25}H_{24}Cl_2F_3N_2O_7$). Modelos de simulação *in silico* foram essenciais para a identificação dos metabólitos e se mostraram um valioso complemento aos experimentos *in vitro*. Os ensaios permitiram, além da identificação, a determinação da taxa de formação dos metabólitos, revelando diferenças significativas entre as espécies, especialmente para os metabólitos conjugados.

Palavras-chave: dapaconazol, imidazol, metabolismo *in vitro*, microssomo, fenotipagem enzimática, anticorpos inibidores, predição *in silico*.

RESUMEN

Las infecciones fúngicas superficiales han aumentado significativamente en las últimas décadas, convirtiéndose en una de las formas de infección más prevalentes. La resistencia fúngica a los compuestos azólicos ha sido un foco importante de investigación en los últimos años. El dapaconazol, un nuevo imidazol antifúngico, se desarrolló mediante innovación radical y ha demostrado eficacia contra hongos patógenos. El objetivo de este estudio fue dilucidar los principales metabolitos generados por el metabolismo de fase I y fase II del dapaconazol in vitro, utilizando microsomas hepáticos humanos (HLM) y de rata (RLM) y herramientas in silico (software Meteor Nexus y GastroPlus®). Las isoenzimas implicadas en el proceso también se investigaron mediante fenotipado enzimático con anticuerpos inhibidores contra las isoenzimas del CYP450. La identificación de los metabolitos se realizó mediante cromatografía líquida cuadrupolo-espectrometría de masas de tiempo de vuelo (LC-QTOF-MS). Para la fenotipificación enzimática, se empleó un método de cromatografía líquida y espectrometría de masas cuadrupolo (LC-MS/MS). Se encontró un total de siete metabolitos en HLM y RLM, de los cuales cinco ($C_2H_{12}Cl_2F_3N_2O$, $C_{12}H_{12}Cl_2F_3N_2O2$, $C_{12}H_{12}Cl_2F_3N_2O2$, $C_{12}H_{12}Cl_2F_3N_2O2$) se produjeron mediante reacciones de fase I y fueron metabolizados por diversas isoenzimas del CYP450 (CYP1A1, CYP1A2, CYP2B6, CYP2C8, CYP2C19, CYP2D6, CYP2E1 y CYP3A4), uno por las fases I y II ($C_2H_{22}Cl_2F_3N_2O8$) y uno directamente por la fase II ($C_2H_{22}Cl_2F_3N_2O7$). Los modelos de simulación in silico resultaron relevantes para la identificación de metabolitos y demostraron ser un complemento importante para los experimentos in vitro. Los ensayos permitieron determinar no solo la tasa de formación de metabolitos, sino también la tasa de formación de los mismos. Se observaron diferencias en la tasa de formación metabólica entre especies, principalmente para los metabolitos conjugados.

Palabras clave: dapaconazol, imidazol, metabolismo *in vitro*, microsoma, fenotipado enzimático, anticuerpos inhibidores, predicción *in silico*.

1 INTRODUCTION

Azole antifungals constitute an essential pharmacological class in the treatment of

systemic and topical fungal infections. The structure of these compounds is defined by a nitrogen-containing heterocyclic azole ring (Allen *et al.,* 2015; Nett; Andes, 2016). Their mechanism of action is based on the inhibition of the enzyme lanosterol 14α-demethylase (CYP51), which belongs to the cytochrome P450 (CYP450) family. This inhibition disrupts the synthesis of ergosterol, an essential component of the fungal plasma membrane, leading to alterations in its permeability and cellular integrity (Allen *et al*., 2015; Bodey, 1992; Gagliano-J *et al*., 2014; Nett; Andes, 2016; Warrilow *et al*., 2016).

Among the topical infections treatable with azoles, cutaneous and nail mycoses are noteworthy, with their prevalence having increased significantly in recent decades (Havlickova *et al.,* 2008). Fungal resistance to this class of compounds is a growing concern, driving the development of new antifungal agents (Canuto; Rodero, 2002; Gagliano-J *et al.,* 2014). In this context, Biolab Sanus Farmacêutica Ltda. developed Zilt®, a cream containing 2.0% dapaconazole tosylate, a new azole imidazole, chemically described as 1-(2-(2,4-dichlorophenyl)-2-(4-(trifluoromethyl)benzyloxy)ethyl)-1H-imidazole, CAS 1269726-67-1, with the molecular formula $C_{19}H_{15}Cl_2F_3N_2O$ and a molecular weight of 414.0514 Da (Antunes *et al*., 2022).

Figure 1. Molecular structure of dapaconazole.

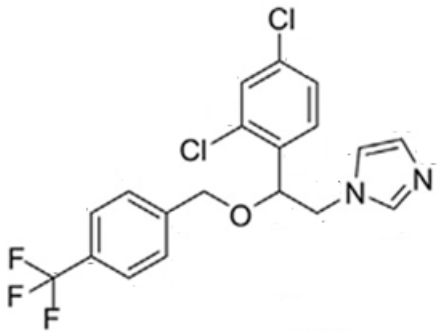

Source. Figure adapted from Antunes *et al*., 2022.

Non-inferiority studies have shown that dapaconazole is not inferior to ketoconazole in the treatment of *Pityriasis versicolor* and *Tinea pedis* and is not inferior to miconazole in the treatment of *Tinea pedis*, with good safety and tolerability profile (Gobbato *et al.,* 2015; Gobbato *et al.,* 2018; Gobbato *et al.*, 2019).

Pharmacokinetic studies conducted in humans with the administration of Zilt® 2% have demonstrated that dapaconazole exhibits a low level of systemic exposure and a favorable safety profile (Gagliano-J *et al*., 2014). In a phase I study, the topical administration of dapaconazole at doses ranging from 0.5 mg to 250 mg resulted in plasma concentrations

comparable to those observed with other topical azole antifungals (De Moraes *et al*., 2014).

Drug metabolism is crucial in preclinical development, influencing the pharmacokinetics and toxicity potential of compounds (Barreiro *et al.,* 1996). Phase I metabolism involves microsomal enzymes, primarily CYP450, which catalyze oxidation, reduction, and hydrolysis reactions. In phase II, conjugation reactions such as glucuronidation (UGT), sulfation (SULT), and glutathione (GST) increase the polarity of metabolites to facilitate renal excretion (Dudda; Kuerzel, 2013; Nagar *et al*., 2014). Furthermore, the investigation of potential drug interactions involving CYP450 inhibition is crucial in the development of azole antifungals (Brüggemann *et al.,* 2009).

Isolated hepatocytes and microsomal fractions are used for studying hepatic metabolism. Microsomal assays are widely employed due to their low cost and ease of use, requiring precise control of variables such as temperature, pH, and cofactors, which are well-established for both metabolic phases (Dudda; Kuerzel, 2013; Gómez-Lechón *et al.,* 2004).

The *in vitro* metabolism of dapaconazole was previously performed by our research group using male Sprague Dawley rats (RLM), male Beagle dogs (BLM), and humans (HLM) liver microsomes. Dapaconazole *in vitro* metabolism demonstrated high metabolic stability in RLM, BLM, and HLM. Three metabolites produced by phase I oxidation reactions were elucidated, keto-dapaconazole ($C_{19}H_{16}Cl_2F_3N_2O_2^+$, *m/z* 431.0545 Da), ester-dapaconazole ($C_{19}H_{14}Cl_2F_3N_2O_2^+$, *m/z* 429.0377 Da), and methylene-dapaconazole ($C_{20}H_{18}Cl_2F_3N_2O^+$, *m/z* 429.0743 Da) (Antunes *et al.*, 2022). Dapaconazole presented a potential for inhibition of all investigated CYP450 isoforms. It is a weak inhibitor of CYP1A2 and CYP2C9, a moderate inhibitor of CYP2C8 and CYP2D6, and a strong inhibitor of CYP2C19 and CYP3A (Antunes *et al.,* 2023).

In vitro enzyme phenotyping allows the identification of the enzymes that contribute to drug metabolism, helping in drug interaction evaluation (Zientek; Youdim, 2015). The main approaches in enzyme phenotyping include the use of monoclonal antibodies, recombinant CYP450 enzymes, and chemical inhibitors in human microsomes (Lu *et al.,* 2003).

Reactions using specific monoclonal antibodies aim to selectively inhibit a CYP450 isoform. By incubating these antibodies with human liver microsomes, a reduction in the formation of drug metabolites can be observed. If the inhibition is significant, it indicates that the inhibited isoform is the main responsible for the drug's metabolism. The precision of monoclonal antibodies, in the case of significant inhibition, makes this approach reliable and can be used as a standalone method, as it avoids cross-reactions with other isoforms (Lu *et al.,* 2003).

To better understand the dapaconazole metabolism, in this study, the main dapaconazole metabolites generated by phase I and phase II metabolism were identified using HLM and RLM. Furthermore, the CYP450 isoenzymes involved in the process were determined by enzyme phenotyping with inhibitory antibodies against some CYP450 isoenzymes. The metabolite identification was performed by liquid chromatography-tandem high-resolution mass spectrometry (LC-HRMS). The determination of dapaconazole for enzyme phenotyping was carried out using liquid chromatography-tandem mass spectrometry (LC-MS/MS) method. I*n silico* predictions of metabolites were also performed to guide the *in vitro* evaluation.

2 MATERIALS AND METHODS

The protocols used in this study were developed based on the adaptation of methods presented by Antunes *et al.* (2022), Godoi *et al*. (2024), and Yan; Caldwell (2013), following the good practice recommendations for drug metabolism studies outlined by Jia; Liu (2007) and the harmonized guideline Guideline on Drug Interaction Studies, ICH M12 (2024) (Antunes *et al.,* 2022; Godoi *et al*., 2024; Yan; Caldwell*,* 2013; Jia; Liu, 2007; ICH M12, 2024).

2.1 *IN SILICO* PREDICTION OF DAPACONAZOLE METABOLISM

Two softwares were used for *in silico* metabolic prediction of dapaconazole. The first software was Meteor Nexus (version 3.1.0, Lhasa Limited, Leeds, United Kingdom) knowledge-based expert systems (Knowledge Bases: Meteor KB 2015 1.0.0), accessed through a trial license. The prediction parameters were set as follows: Amplitude First (breadth first) for processing direction; growth from phase II products to phase restriction; limited metabolite cycles with a maximum depth of 3; metabolism site score (with molecular mass variation) with molecular mass similarity limit of 70, score filter set as "relative" and score limit set to 70. The following reactions considered for the phase I metabolism were oxidation, reduction, hydrolysis, dehydration, hydration, hydrolytic and non-hydrolytic fragmentation or ring-opening, ring closure, and decarboxylation. The reactions considered for phase II metabolism were O-glucuronidation, N-glucuronidation, S-glucuronidation and glucuronidations involving alkyl halides, halogenated alkenes, alkynes, esters, epoxides, episulfides, arenes oxides, and oxi-conjugates.

The second software used was GastroPlus® version 10.1 (Simulations Plus Inc., Lancaster, CA, USA), with the ADMET Predictor® module (version 12.0) and MedChem

Designer® module (version 8.0), academic license by Simulations Plus. For ADMET Predictor, only one metabolic cycle was selected, with phase I reaction enzymes: CYP1A2, CYP2A6, CYP2B6, CYP2C8, CYP2C9, CYP2C19, CYP2D6, CYP2E1, CYP3A4, and AOX; and phase II reaction enzymes: UGT1A1, UGT1A3, UGT1A4, UGT1A6, UGT1A8, UGT1A9, UGT1A10, UGT2B7, and UGT2B15. The MedChem Designer® (version 8.0) module was employed for obtaining the chemical structures and identifiers (SMILES) of the metabolites.

2.2 CHEMICAL PRODUCTS AND REAGENTS

Dapaconazole (free base) was provided by Biolab Farmacêutica Ltda. (São Paulo, Brazil). Verapamil, used as the internal standard (IS) for the enzyme phenotyping reaction, was purchased from Sigma-Aldrich (St. Louis, MI, USA). The Corning® Gentest™ Phosphate Buffer, 0.1 M, pH 7.4, reduced nicotinamide adenine dinucleotide phosphate (NADPH) regenerating system solutions A (26 mmol/L $NADP^+$, 66 mmol/L glucose-6-phosphate and 66 mmol/L $MgCl_2$) and B (40 U/mL glucose-6-phosphate dehydrogenase in 5 mmol/L sodium citrate) were purchased from Corning (Woburn, MA, USA). Methanol, acetonitrile, uridine 5'-diphosphoglucuronic acid trisodium salt (UDPGA), adenosine 3'-phosphate 5'-phosphosulfate triethylammonium salt (PAPS), S-(5'-adenosyl)-L-methionine p-toluenesulfonate salt (SAM) were purchased from Sigma-Aldrich (St. Louis, MI, USA), along with monoclonal antibodies Anti-CYP3A4, Anti-CYP2E1, Anti-CYP2C19, Anti-CYP2B6, Anti-CYP1A2, Anti-CYP2C8, Anti-CYP2D6, and Anti-CYP1A1. Ultra-pure water was obtained through a Mili-Q RG system from Millipore (Burlington, MA, USA). LC/MS-grade water and LC/MS-grade methanol were purchased from Merck (Darmstadt, Germany).

2.3 PREPARATION OF STOCK SOLUTIONS AND MICROSOMES

Dapaconazole was prepared at 24.1 mM (10 mg/mL) in methanol for the metabolic identification assay. Verapamil, used as internal standard (IS), was prepared at 1.28 µM (0.6 mg/mL) in acetonitrile.

HLM containing 20 mg/mL of microsomal proteins and 270 pmol of CYP450/mg protein, were obtained from Sigma-Aldrich and stored at −80 °C until use.

The pooled RLM used were prepared by differential ultracentrifugation and quantified by Bradford's method (1976) (Bradford, 1976; Jia; Liu *et al*., 2007, Pearce *et al*., 1996). The livers used in this study were sourced from control and healthy animals sacrificed for other

experiments related to projects from the Pharmacology Postgraduate Program at UNICAMP. The microsome preparation process involved removing the liver from five Wistar rats (Ethical Committee for Animal Research at the State University of Campinas – CEUA/UNICAMP protocol numbers 5987-1/2022 and 5865-1/2022) and adding them to a Tris-HCl buffer (50 mM, pH 7.4) with KCl (150 mM). The livers were chopped and washed three times with the buffer solution. Twenty milliliters of buffer were added to the liver slices for homogenization using a Potter-type homogenizer (3 cycles at 1,000 rpm for 1 minute). The homogenate was centrifuged at 10,000 × *g* for 15 minutes at 4 °C. The supernatant was then ultracentrifuged at 100,000 × *g* for 60 minutes at 4 °C to obtain the microsomal pellet. The microsomal pellet was resuspended in HEPES-HCl buffer (50 mM, pH 7.4) containing 20 % glycerol and 1 mM EDTA.

2.4 INCUBATION OF DAPACONAZOLE FOR METABOLITE IDENTIFICATION

Incubations were performed with phase I, phase II, and phase I + II reactions. In phase II, metabolites generated directly by conjugation reactions were evaluated, and in phase I + II, the phase II-conjugated metabolites that were initially substrates of phase I reactions were evaluated.

In all reactions, 30 µL of the dapaconazole stock solution (10 mg/mL) were initially added to 1.5 mL propylene tubes and evaporated under a nitrogen stream. For the phase I reactions, NADPH regeneration system solution A (25 µL) and solution B (5 µL), ultrapure water (20 µL), and phosphate buffer (100 mM, 100 µL) were added (final volume of 150 µL). For the phase II reactions, the phase II cofactors (10 µL of PAPS 0.49 mM, 10 µL of SAM 3.79 mM, and 1.75 mg of UDPGA 13.70 mM), ultrapure water (20 µL), and phosphate buffer (100 mM 108 µL) were added (final volume of 150 µL). Finally, for the phase I + phase II reactions, the same preparation steps as those for phase I were followed, adding the phase II cofactors, 20 µL of ultrapure water, and 78 µL of phosphate buffer, 100 mM (final volume of 150 µL).

The solutions were pre-incubated for 5 minutes in a shaker incubator model MTC 100 (Miulab, Zhejiang, China) at 500 rpm and 37 °C. To initiate the reactions, 50 µL of HLM and RLM at a concentration of 20 mg/mL of proteins were added to all pre-incubated shaking tubes. Phase I incubations were evaluated at 0, 15, 30, 60, and 120 minutes. Phase II and phase I + II incubations were evaluated at 0 and 120 minutes. The enzymatic reactions were stopped by adding 250 µL of ice-cold acetonitrile. The samples were then vortexed for 5 minutes using a BenchMixer™ XL model (Benchmark, New Jersey, USA) and centrifuged at 12,000 x *g* for 15

minutes at 4 °C in a refrigerated centrifuge model Hettich® Universal 320 R (Tuttlingen, Germany). The supernatants were transferred to 1.5 mL vials, and 4 µL were injected into the LC-HRMS system.

2.5 INCUBATION OF DAPACONAZOLE FOR ENZYMATIC PHENOTYPING REACTION

The reactions were performed in triplicate (Yan; Caldwell, 2013), considering a final incubation volume of 300 µL and 0.5 mg/mL of HLM, for 8 monoclonal antibodies: anti-CYP3A4 (0.77 mg/mL), anti-CYP2E1 (0.1 mg/mL), anti-CYP2C19 (0.1 mg/mL), anti-CYP2B6 (0.05 mg/mL), anti-CYP1A2 (1 mg/mL), anti-CYP2C8 (0.1 mg/mL), anti-CYP2D6 (1 mg/mL), and anti-CYP1A1 (1 mg/mL). The antibodies were selected based on the main isoenzymes of the CYP450 system and the enzymatic inhibition reactions of dapaconazole reported by Antunes *et al.* (2022). The dilutions were performed according to the antibody supplier. Dilutions of 20, 200, and 400 were considered for antibodies with a concentration greater than 0.1 mg/mL, and dilutions of 20, 100, and 200 were considered for antibodies with a concentration less than or equal to 0.1 mg/mL. To calculate the antibody volume in the incubation reactions, the final volume of 300 µL was divided by the value of each dilution factor.

For the incubation reactions, a drug-HLM solution was prepared by pipetting 108.75 µL of the dapaconazole stock solution to achieve a final concentration of 357.9 µM, corresponding to 3x Km of dapaconazole, as reported by Antunes *et al*. (2022) as 119.3 µM (S_{50}). To complete the drug-HLM solution, 500 µL of HLM, 1000 µL of phosphate buffer, and 8500 µL of ultrapure water were also added.

Aliquots of 100 µL of the drug-HLM solution were pipetted into propylene tubes labeled as Anti-CYP3A4, Anti-CYP2E1, Anti-CYP2C19, Anti-CYP2B6, Anti-CYP1A2, Anti-CYP2C8, Anti-CYP2D6, Anti-CYP1A1, and negative control. The corresponding amount of specific antibody, based on the dilution, was added to the tubes, except for the control group, to which the same volume of phosphate buffer was added. The volume was completed with phosphate buffer to a total of 150 µL. The solutions were incubated for 15 minutes at room temperature, followed by a 3-minute water bath. Subsequently, 15 µL of phosphate buffer, 117 µL of ultrapure water, 15 µL of NADP+, and 3 µL of glucose-6-phosphate dehydrogenase were added into each propylene tube, totaling 150 µL of the NADPH regeneration solution. The incubation continued at 37°C for 30 minutes. Then, 150 µL of cold acetonitrile was added to

stop the reaction. The samples were vortexed using the BenchMixer™ XL model (Benchmark, New Jersey, USA) for 10 minutes and centrifuged at 12,000 x *g* for 15 minutes at 4°C in the refrigerated centrifuge Hettich® Universal 320 R (Tuttlingen, Germany). The supernatants were transferred to vials, and 10 µL were injected into the LC-MS/MS system.

2.6 IDENTIFICATION OF DAPACONAZOLE METABOLITES BY LC-HRMS

The identification of the dapaconazol metabolites was performed using a Nexera HPLC (Shimadzu, Kyoto, Japan) chromatographic system coupled to LCMS9030 quadrupole-time-of-flight mass spectrometer (QToF) (Shimadzu, Kyoto, Japan) using an electrospray ionization source operating in positive mode (ESI^+). The chromatographic separation was carried out on a Cortecs T3 C18 column (2.1 x 150 mm, 2.7 µm, Waters), maintained at 40 °C. The mobile phases consisted of LCMS grade water (MPA) and LCMS grade methanol (MPB), both added with 0.1% formic acid, at a flow rate of 0.3 mL/min, with an elution gradient starting at 5% MPB, which was maintained for 1 minute, followed by a linear increase to 95% MPB over 18 minutes, keeping this ratio for 3 minutes, and finally returning to the initial condition in 0.1 minute. The total chromatographic analysis time was 25 minutes. The ESI^+ was employed with a voltage of 4.5 kV, heating gas at 10 L/min, drying gas (air) at 10 L/min, nebulization gas flow (N_2) at 2 L/min, and interface and desolvation line temperatures set to 400 °C and 250 °C, respectively.

The mass spectrometer was set for data-dependent acquisition (DDA) mode, with mass range *m/z* 50-800 for full scan (MS) event and for the top 3 dependent (MS^2), triggering fragmentation events above 3,000 counts of intensity. The collision energy was set in spread mode 30±25 eV. Before data acquisitions, the mass spectrometer was calibrated to ensure mass resolution and accuracy, using a sodium iodide ($Na\text{-}(NaI)_5$) solution as a mass reference standard (monitoring *m/z* 1971.6144), considering a maximum acceptable mass error of 1 ppm and a minimum resolution of 30,000. Data acquisition was performed using LabSolutions software version 5.10 (Shimadzu, Kyoto, Japan), and data processing was carried out with LabSolutions Insight Explore software version 1.0.0.0 (Shimadzu, Kyoto, Japan).

For the identification of dapaconazole and its metabolites, a maximum mass error of 5 ppm was set for the precursor ions and 15 ppm for the products. Additionally, for the characterization of the possible structures of the metabolites, only spectra with at least two ions corresponding to their gas-phase fragmentation mechanisms, in addition to the identification of the precursor itself, were considered. Thus, peaks whose spectra did not meet these acceptance

criteria were excluded from the characterization of potential metabolites. The assignment of the fragments chemical structure of dapaconazole metabolites was assisted using the "Spectra Prediction" tool of the Competitive Fragmentation Modeling for Metabolite Identification (CFM-ID) version 4.0 (Wang *et al*., 2022).

2.7 DETERMINATION OF DAPACONAZOLE METABOLITES FOR THE ENZYME PHENOTYPING BY LC-MS/MS

The determination of dapaconazole metabolites for the enzyme phenotyping assessment was performed using a Nexera HPLC chromatographic system coupled to a LCMS8045 triple quadrupole mass spectrometer (Shimadzu, Kyoto, Japan). Separation was performed using a Raptor^{TM} Biphenyl chromatographic column (2.1 x 100 mm, 2.7 µm) at 40 °C. The chromatographic separation was performed at a flow rate of 0.4 mL/min, employing mobile phases containing 2 mM ammonium formate and 0.1% formic acid in water (MPA) and in methanol (MPB). Chromatographic gradient started at 20% MPB up to 0.2 min, ramping to 95% MPB until 3 min, maintaining this proportion for 3 min and then returning to the initial condition until 6.1 min, maintaining this proportion up to 7 min. The ionization source used was the electrospray operating in positive mode. Data acquisitions were performed in multiple reaction monitoring (MRM) mode. For dapaconazole, a transition of *m/z* 236.1 → *m/z* 188.0 was employed using a collision energy (CE) of 32 eV for dapaconazole monitoring. M1 was monitored using *m/z* 429.0 → *m/z* 159.0 with a CE of 32 eV, and *m/z* 429.0 → *m/z* 241.0 with a CE of 32 eV, for M2 *m/z* 431.0 → *m/z* 159.0 with a CE of 32 eV and *m/z* 431.0 → *m/z* 243.0 with a CE of 32 eV; for M3 *m/z* 257.0 → m/z 125.0 with a CE of 35 eV and *m/z* 257.0 → *m/z* 69.0 with a CE of 35 eV, for M4 *m/z* 431.0 → *m/z* 159.0 with a CE of 35 eV and *m/z* 431.0 → *m/z* 255.0 with a CE of 35 eV, and for M5 *m/z* 429.0 → *m/z* 159.0 with a CE of 35 eV and *m/z* 429.0 → *m/z* 173.0 with a CE of 35 eV. Data acquisition and analysis was performed using LabSolutions software version 5.114 (Shimadzu, Kyoto, Japan).

3 RESULTS AND DISCUSSIONS

3.1 *IN SILICO* PREDICTIONS OF DAPACONAZOLE METABOLISM

The Meteor Nexus software predicted 12 phase I metabolites and 10 phase I + II metabolites. It forecasted reactions such as oxidation, reduction, hydrolysis, dealkylation,

cleavage, sulfonation, glucuronidation, and conjugation. The software ranked the metabolites based on their probability of occurrence, represented by a score. Figure 2 represents the predicted metabolites in descending order of incidence. All the predicted metabolites were screened through the *in vitro* assays using HLM and RLM. Two metabolites, M25 ($C_{11}H_{10}Cl_2N_2O$; exact mass 256.0170 Da) formed by O-dealkylation and M23 ($C_{19}H_{15}Cl_2F_3N_2O_2$; exact mass: 430.0463 Da) were identified in the *in vitro* analysis.

The ADMET Predictor® software predicted 10 phase I metabolites, and one phase II metabolite. The predicted reactions included oxidation, cleavage, hydroxylation, and conjugation. Figures 3 and 4 show the predicted metabolites ranked by incidence, based on the software's algorithm. Among the predicted metabolites, three were identified through *in vitro* analysis: M6 ($C_{19}H_{15}Cl_2F_3N_2O_2$; exact mass 430.0463 Da) formed by an oxidation reaction and M8 formed by oxidative O-dealkylation that caused a cleavage between the alkyl group and the oxygen atom, generating two structures: $C_{11}H_{10}Cl_2N_2O$ with exact mass 256.0170 Da and $C_8H_5F_3O$ with exact mass 174.0292 Da, both metabolites generated by phase I metabolism, and the third metabolite M1 (phase II reaction), $C_{25}H_{23}Cl_2F_3N_2O_7$ and exact mass 590.0834 Da, formed by glucuronidation.

The most frequent reactions, considering the probability of metabolite formation presented by the software were oxidative O-dealkylation and hydroxylation for Meteor Nexus, and oxidative O-dealkylation and oxidation for ADMET Predictor®. To ADMET Predictor®, three metabolites presented two structures, generated by cleavage, which include M8 previously described, M2 ($C_{16}H_{11}Cl_2F_3O_2$, exact mass 362.0088 Da and $C_3H_4N_2$, exact mass 68.0374 Da) and M4 ($C_{11}H_8Cl_2N_2O$, exact mass 254.0014 Da and $C_8H_7F_3O$, exact mass 176.0449 Da), as shown in Figure 3.

In the case of Meteor, three metabolism cycles from phase I and phase II were considered, aiming to extrapolate the largest possible number of reactions, as the objective of the study was metabolic identification. However, it was observed that the probability of identifying metabolites decreases when considering three cycles due to the characteristics of dapaconazole and the reactions involved. For this reason, the ADME Predictor® was used to predict reactions considering only one metabolism cycle, so that more reactions could be predicted using two different bases.

Interestingly, only one metabolite was predicted by both software: M8 of ADMET Predictor®, which corresponds to M25 from the Meteor Nexus database. This metabolite was identified and was the fourth most abundant in HLM and RLM at all incubation times.

Figure 2. *In silico* predictions obtained from Meteor Nexus (version 3.1.0, Lhasa Limited, Leeds, United Kingdom) software, presented by the incidence of metabolite formation.

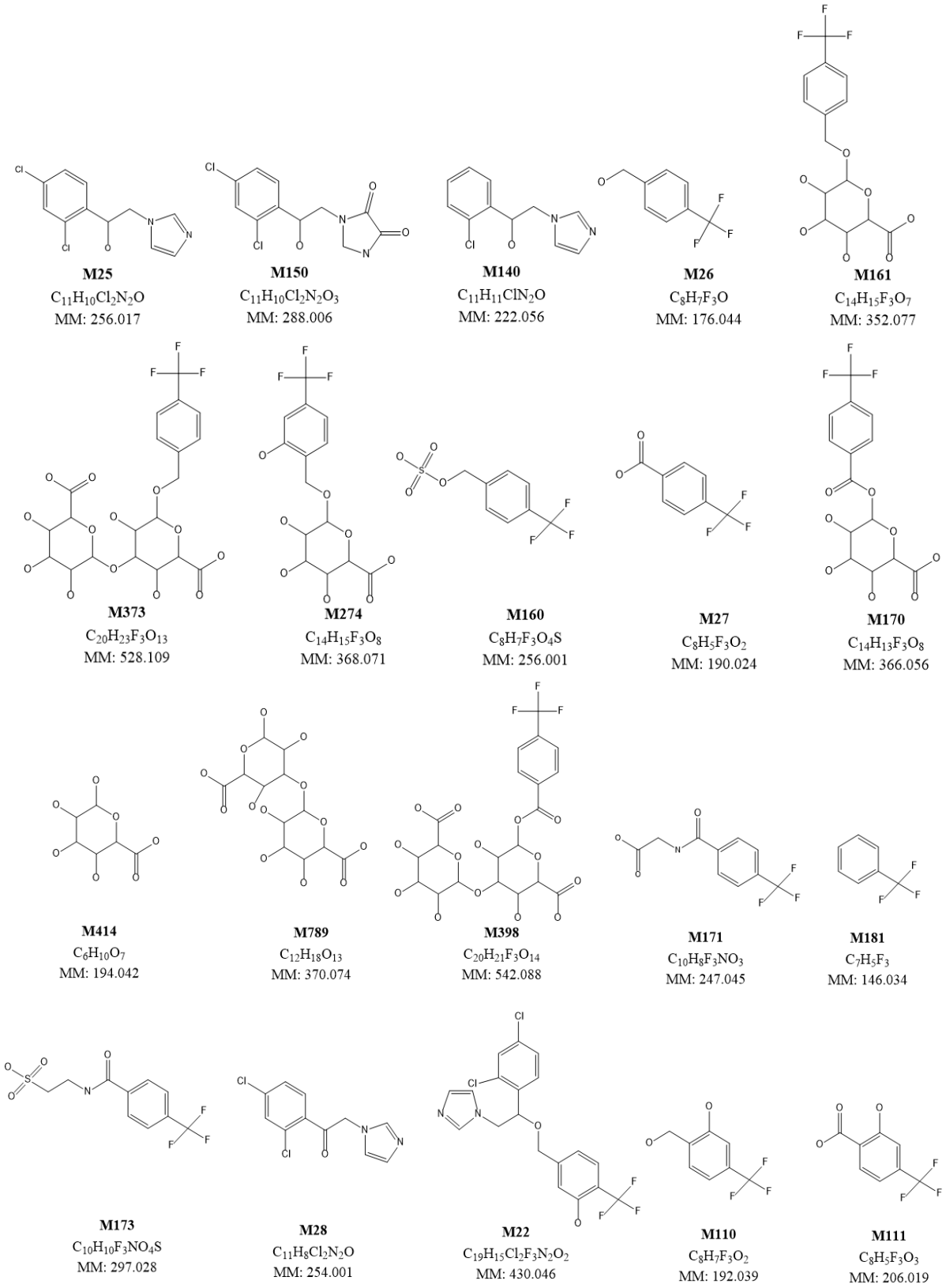

Source. Repository originating from the essay conducted by the authors.

Figure 3. *In silico* predictions obtained from Meteor Nexus (version 3.1.0, Lhasa Limited, Leeds, United Kingdom) software, presented by the incidence of metabolite formation. (Continuation).

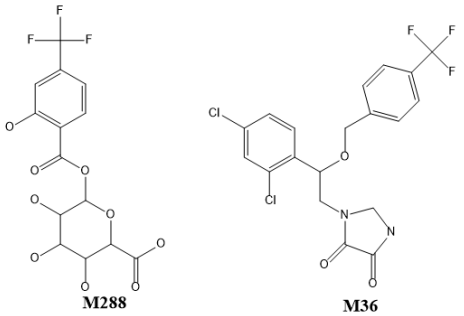

Source. Repository originating from the essay conducted by the authors.

Figure 4. In silico predictions obtained from GastroPlus® version 10.1 (Simulations Plus Inc., Lancaster, CA, USA), ADMET Predictor® version 12.0 module for dapaconazole metabolism prediction, and MedChem Designer® version 8.0 module for assisting in obtaining chemical structures, formulas, and identifiers (SMILES), presented by the incidence of formation of phase I metabolites.

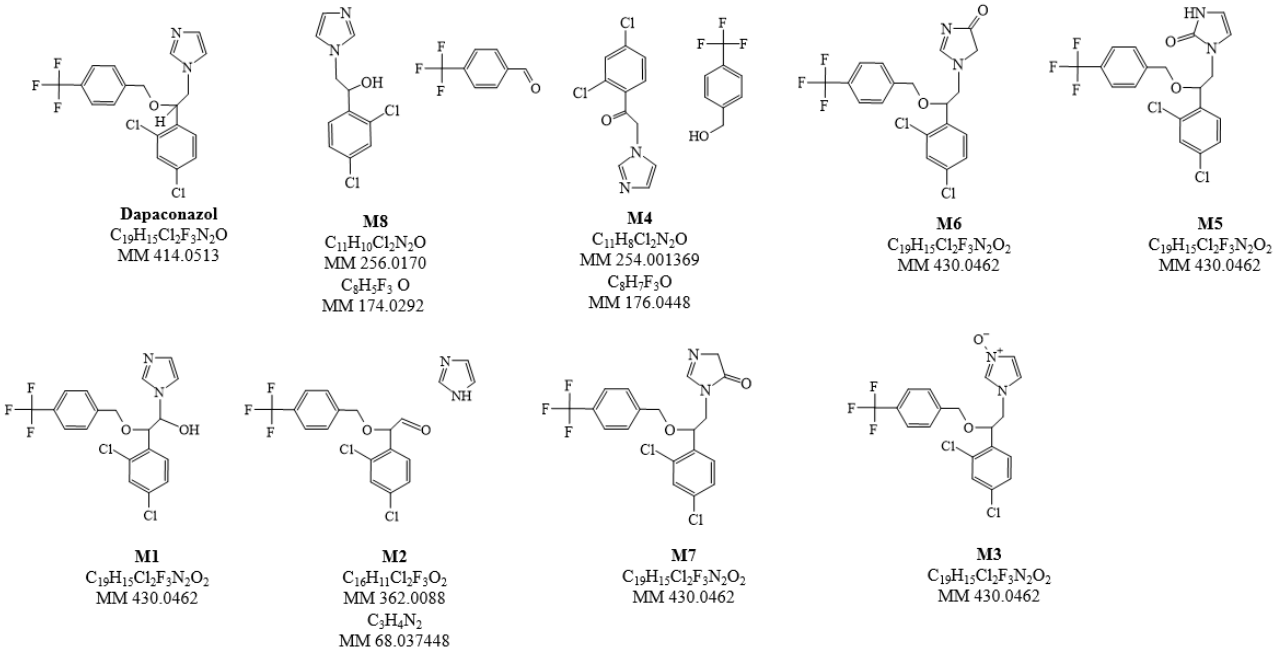

Source. Repository originating from the essay conducted by the authors.

Figure 5. *In silico* predictions obtained from GastroPlus® version 10.1 (Simulations Plus Inc., Lancaster, CA, USA), with the ADMET Predictor® module (version 12.0) and MedChem Designer® module (version 8.0) for assisting in obtaining chemical structures, formulas, and identifiers (SMILES), presented by the incidence of formation of phase II metabolites.

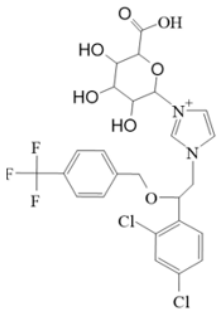

M1
$C_{25}H_{24}Cl_2F_3N_2O_{7+}$
MM 591,0912

Source. Repository originating from the essay conducted by the authors.

3.2 IDENTIFICATION OF DAPACONAZOLE AND ITS METABOLITES

Dapaconazole and the predicted metabolites were screened by LC-QTOF in the *in vitro* experiments. We expected to find the product ion profile of the protonated molecule, in ESI^+ mode. In the metabolic identification assay, dapaconazole and five phase I metabolites were identified, corresponding to the following metabolic reactions: methylation (M1, $C_{20}H_{18}Cl_2F_3N_2O$; exact mass 429.0748 Da), oxidation of the imidazole ring (M2, $C_{19}H_{16}Cl_2F_3N_2O_2$; exact mass 431.0540 Da), oxidative O-dealkylation (M3, $C_{11}H_{11}Cl_2N_2O$; exact mass 257.0248 Da), hydroxylation (M4, $C_{19}H_{16}Cl_2F_3N_2O_2$; exact mass 431.0540 Da), and aliphatic oxidation (M5, $C_{19}H_{14}Cl_2F_3N_2O_2$; exact mass 429.0384 Da). One phase I + II metabolite was identified (M6, $C_{25}H_{24}Cl_2F_3N_2O_8$; exact mass 607.0861 Da), produced by a hydroxylation followed by a glucuronidation reaction. Moreover, one phase II metabolite was identified, which was produced by a glucuronidation reaction (M7, $C_{25}H_{24}Cl_2F_3N_2O_7$; exact mass 591.0912 Da).

To define the methylation site of M1 with a protonated molecular ion of *m/z* 429.07507, the mass of a methyl group was hypothetically added to dapaconazole fragments, as shown in Figure 5. The presence of the fragment *m/z* 241.09498 in MS^2 spectra of M1 characterizes the insertion of a methylene in the fragments with *m/z* 227.07905 of dapaconazole, as displayed in Figure 6A. The addition of a methyl group in other dapaconazole fragments was not observed, reinforcing the specificity of the methylation insertion site. The imidazole ring contains two nitrogen atoms, one of which is basic (with a lone pair of electrons) and the other involved in resonance. This structure provides different positions susceptible to chemical substitution. This

metabolite has previously been described by Antunes *et al.* (2022) as methylene-dapaconazole, reinforcing the relevance of this metabolic transformation in dapaconazole derivatives.

The same process was performed to M2, with a protonated molecular ion of *m/z* 431.05384. The presence of the fragment *m/z* 243.07436 in MS^2 spectra of M2 characterizes the insertion of the oxygen in the fragments with *m/z* 227.07905 of dapaconazole, as displayed in Figure 6B. The addition of oxygen in the fragment with *m/z* 69.04425 of dapaconazole, reinforces the specificity of the oxidation of the imidazole ring, corresponding to the fragment *m/z* 85.04051 of M2. The carbons at the C2, C4, and C5 positions of the imidazole ring are susceptible to oxidation due to resonance with the nitrogen atoms, which makes these positions vulnerable to oxygen addition reactions. During the chromatographic analysis in the metabolic identification assay, M2 showed two distinct chromatographic peaks (peak 1 and peak 2). These peaks suggest the presence of positional isomers, which differ in the location of the oxygen in the molecule. The metabolite M2 corresponds to M6 of the ADMET Predictor®. This metabolite has previously been described by Antunes *et al*. (2022) as keto-dapaconazole.

M3 is proposed to be formed through the oxidative metabolism of dapaconazole, involving a C–O cleavage mechanism, producing a protonated molecular ion of *m/z* 257.02435 as demonstrated in Figure 6C. The fragmentation pathways observed in the MS2 spectrum of M3 provide further insights into its structural modification. The presence of the fragment ion at *m/z* 223.06529 suggests the loss of a chlorine atom from the 1,3-dichlorobenzene moiety, resulting a decreasing of 33.9610 Da. Additionally, the characteristic fragment at *m/z* 125.01535 corresponds to a cleavage at the aromatic region, yielding a stable cationic species. The imidazole-derived fragment at *m/z* 69.04462 further supports the metabolic oxidation occurring at a specific site while preserving the core scaffold of dapaconazole. M3 corresponds to M25 of Meteor and M8 of the ADMET Predictor® database.

To define the hydroxylation site of M4 with *m/z* 431.05407, the presence of the fragment *m/z* 255.00882 in MS^2 spectra of M4 characterizes the insertion of the hydroxyl group in the fragments with *m/z* 239.01360, as displayed in Figure 6D. The addition of the hydroxyl group in other dapaconazole fragments was not observed, reinforcing the specificity of the hydroxylation insertion site. The metabolite M4 corresponds to M23 of Meteor database. During the chromatographic analysis in the metabolic identification assay, M4 showed three distinct chromatographic peaks. These peaks suggest the presence of positional isomers, which differ in the location of the hydroxyl group in the 1,3-dichlorobenzene ring.

M5 was detected with *m/z* 429.03967 (Figure 6E), corresponding to an esther-dapaconazole derivative formed through keto-type oxidation. This oxidative modification

likely results in the insertion of an oxygen atom, leading to ester formation. The presence of the fragment ion at *m/z* 173.02155 suggests oxidation occurring in the trifluorophenyl moiety, reinforcing the site specificity of the modification. This fragment likely arises from heterolytic cleavage between O-9 and C-8, generating an oxonium ion. Additionally, the ion at *m/z* 159.04184, corresponding to the trifluorobenzyl cation, further supports the structural assignment of M5. This metabolite has previously been described by Antunes *et al.* (2022) as esther-dapaconazole.

M6 was detected at *m/z* 607.08680. The presence of the fragment *m/z* 431.05430 in MS^2 spectra characterizes the insertion of the hydroxyl group in the dapaconazole with *m/z* 415.05923, as displayed in Figure 7A. When the hydroxyl group is added to the fragment *m/z* 227.07905 of dapaconazole, the fragment *m/z* 243.074500 is found, just as when the hydroxyl group is added to the fragment *m/z* 69.04425, the fragment *m/z* 85.03970 is found, inferring that hydroxylation occurs in the imidazole ring. Since this is a phase I + II metabolite, it is expected that the glucuronide will be inserted into the hydroxyl group added to the imidazole ring. The imidazole ring contains two nitrogen atoms and carbons that are susceptible to insertion of oxygen (hydroxylation). The basic nitrogen (with a lone pair of electrons) and the resonance between the atoms of the ring make certain positions more reactive for modifications such as hydroxylation. Additionally, the presence of an oxygen atom makes the hydroxyl group suitable for undergoing a reaction with glucuronic acid in a conjugation process. During the chromatographic analysis in the metabolic identification assay, M6 showed three distinct chromatographic peaks. These peaks suggest the presence of positional isomers, which differ in the location of the hydroxyl in the molecule.

Considering the same rationale for glucuronidation in the imidazole ring, which has several reactive positions due to its structure, with the presence of nitrogen capable of donating electrons, when the glucuronide is inserted into dapaconazole, the metabolite M7 exhibiting *m/z* 591.09222 was found (Figure 7B). Other locations of the molecule sterically hinder the binding. The insertion of the glucuronide into the imidazole ring for M7 was predicted by the GastroPlus® software.

Figures 5 to 7 present the MS^2 mass spectra of dapaconazole and the identified metabolites, with electrospray ionization in positive mode obtained in the identification experiment in HLM by LC-HRMS. Table 1 lists the molecular and analytical information for dapaconazole and the metabolites identified in HLM and RLM.

Figure 6. MSMS mass spectrum of dapaconazole with electrospray ionization in positive mode obtained in the identification experiment in human liver microsomes (HLM) by LC-HRMS (theoretical exact *m/z* 415.05918).

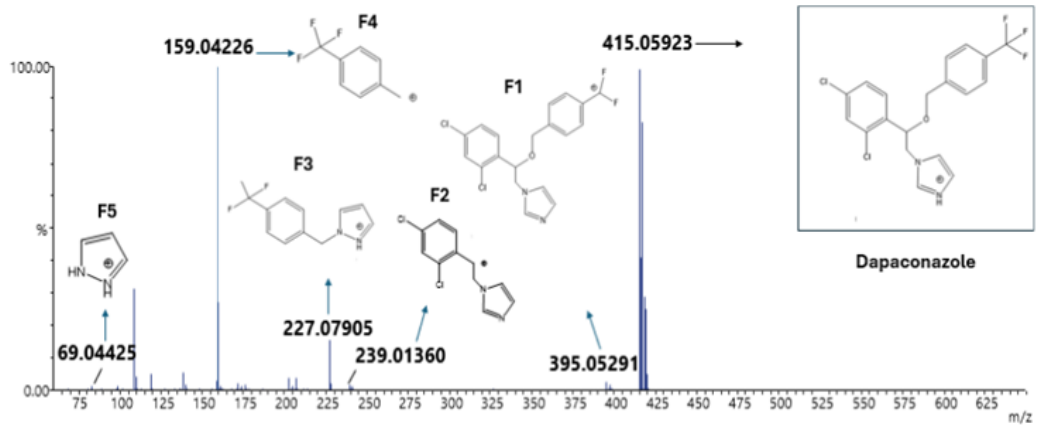

Source. Repository originating from the essay conducted by the authors.

Figure 7. Mass spectrum obtained in the metabolite identification experiment - Phase I reactions (M1 to M5), with electrospray ionization in positive mode obtained in the identification experiment in human liver microsomes (HLM) by LC-HRMS.

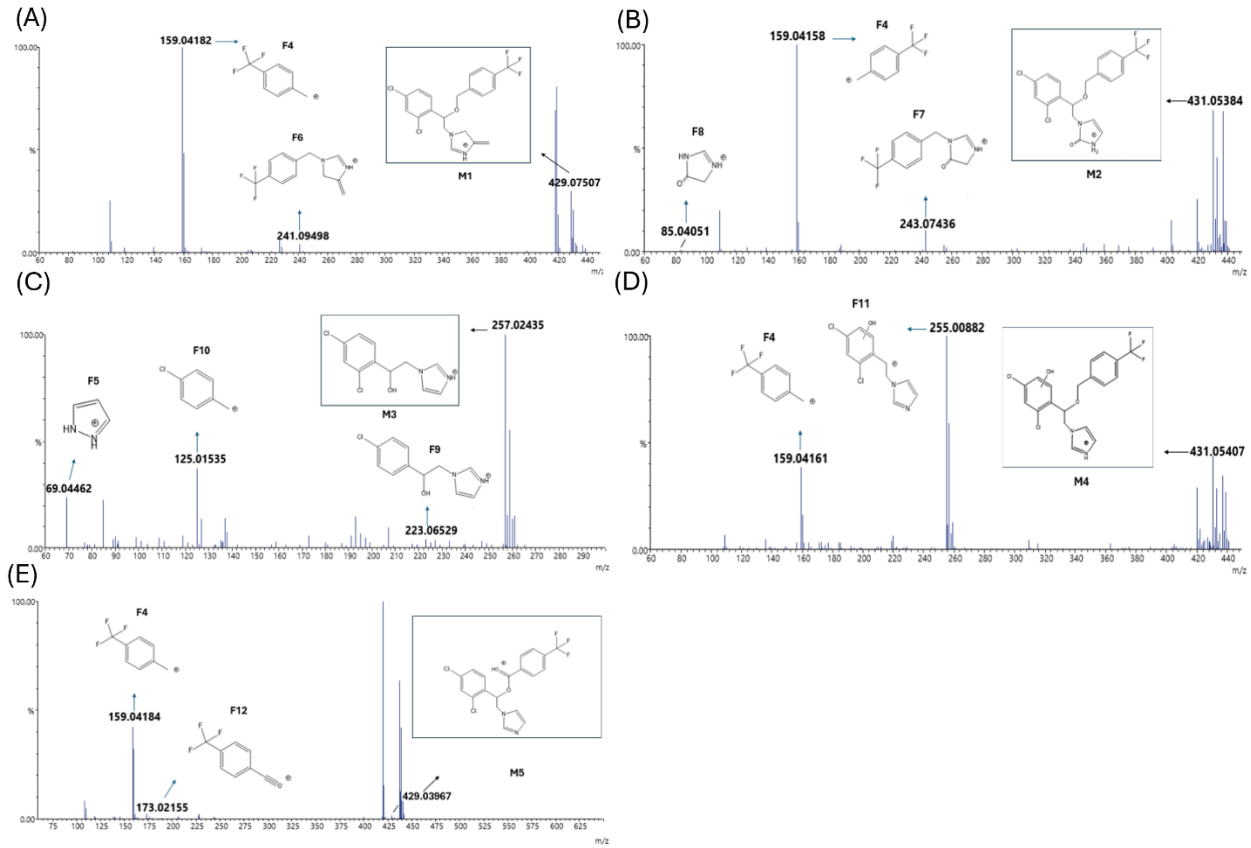

Caption:(A): M1, (B): M2, (C): M3, (D): M4, (E): M5.
Source. Repository originating from the essay conducted by the authors.

Figure 8. Mass spectrum obtained in the metabolite identification experiment - Phase I + II and II reactions (M6 and M7), with electrospray ionization in positive mode obtained in the identification experiment in human liver microsomes (HLM) by LC-HRMS.

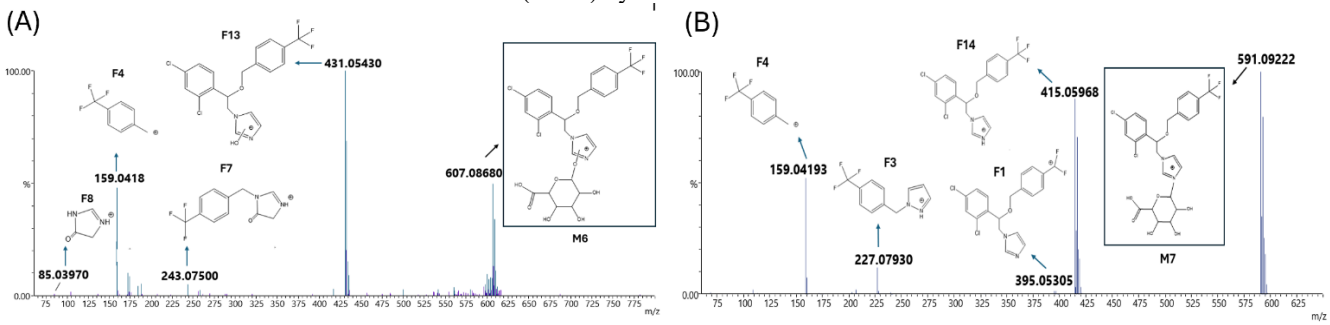

Caption:(A): M6, (B): M7.
Source. Repository originating from the essay conducted by the authors.

Table 1. Analytical and molecular information of dapaconazole and metabolites in human (HLM) and rat (RLM) liver microsomes.

Molecule	Metabolic Reaction	Fragment	Molecular Formula	Theoretical Exact Mass $[M+H]^+$	Exact Mass Measured $[M+H]^+$	Mass Error (ppm)	Retention Time (min)
Dapaconazole	-	-	$C_{19}H_{16}Cl_2F_3N_2O$	415.05918	415.05923	-0.13	13.24
		F1	$C_{19}H_{15}Cl_2F_2N_2O$	395.05295	395.05291	0.10	
		F2	$C_{11}H_9N_2Cl_2$	239.01428	239.01360	2.84	
		F3	$C_{11}H_{10}N_2F_3$	227.07961	227.07905	2.45	
		F4	$C_8H_6F_3$	159.04216	159.04226	-0.64	
		F5	$C_3H_5N_2$	69.04527	69.04425	14.82	
M1	Methylenation	-	$C_{20}H_{18}Cl_2F_3N_2O$	429.07483	429.07507	-0.56	13.18
		F6	$C_{12}H_{12}N_2F_3$	241.09526	241.09498	1.15	
		F4	$C_8H_6F_3$	159.04216	159.04182	2.13	
M2	Imidazole oxidation	-	$C_{19}H_{16}Cl_2F_3N_2O_2$	431.05409	431.05384	0.59	14.57 (peak 1)
		F7	$C_{11}H_{10}N_2OF_3$	243.07452	243.07436	0.67	15.52 (peak 2)
		F4	$C_8H_6F_3$	159.04216	159.04158	3.64	
		F8	$C_3H_5N_2O$	85.04019	85.04051	-3.79	
M3	Oxidative O-dealkylation	-	$C_{11}H_{11}Cl_2N_2O$	257.02484	257.02435	1.92	6.62
		F9	$C_{11}H_{12}ClN_2O$	223.06382	223.06529	-6.61	
		F10	C_7H_6Cl	125.01580	125.01535	3.62	
		F5	$C_3H_5N_2$	69.04527	69.04462	9.46	
M4	Hydroxylation	-	$C_{19}H_{16}Cl_2F_3N_2O_2$	431.05409	431.05407	0.05	14.50 (peak 1)
		F11	$C_{11}H_9Cl_2N_2O$	255.00919	255.00882	1.47	15.40 (peak 2)
		F4	$C_8H_6F_3$	159.04216	159.04161	3.45	16.24 (peak 3)
M5	Keto-type oxidation	-	$C_{19}H_{14}Cl_2F_3N_2O_2$	429.03844	429.03967	-2.86	12.97
		F12	$C_8H_4OF_3$	173.02142	173.02155	-0.73	
		F4	$C_8H_6F_3$	159.04216	159.04184	2.01	
M6	Hydroxylation + glucuronidation	-	$C_{25}H_{24}Cl_2F_3N_2O_8$	607.08618	607.08680	-1.02	12.50 (peak 1)
		F13	$C_{19}H_{16}Cl_2F_3N_2O_2$	431.05409	431.05430	-0.48	13.15 (peak 2)
		F7	$C_{11}H_{10}N_2OF_3$	243.07452	243.07500	-1.97	14.50 (peak 3)
		F4	$C_8H_6F_3$	159.04216	159.04180	2.26	
		F8	$C_3H_5N_2O$	85.04019	85.03970	5.76	
M7	Glucuronidation	-	$C_{25}H_{24}Cl_2F_3N_2O_7$	591.09127	591.09222	-1.61	13.18
		F14	$C_{19}H_{16}Cl_2F_3N_2O$	415.05918	415.05968	-1.21	
		F1	$C_{19}H_{15}Cl_2F_2N_2O$	395.05295	395.05305	-0.25	

F3	$C_{11}H_{10}N_2F_3$	227.07961	227.07930	1.35
F4	$C_8H_6F_3$	159.04216	159.04193	1.44

Source. Repository originating from the essay conducted by the authors.

3.3 FORMATION RATE OF THE IDENTIFIED METABOLITES

The most abundant phase I metabolites in HLM and RLM are M1, M4, and M2 respectively, followed by M3 and M5. When comparing the formation rate of phase I metabolites over the incubation time, considering the total metabolite area versus individual areas, and in the case of more than one chromatographic peak, the sum of all peak areas was performed, M1 represented 71.03% of the formation rate at 15 min, 70.74% at 30 min, 60.69% at 60 min, and 56.23% at 120 min for HLM, and 61.2%, 60.02%, 45.89%, and 32.84% for RLM, respectively. M4 represented 10.92% at 15 min, 11.78% at 30 min, 16.49% at 60 min, and 17.14% at 120 min for HLM, and 14.24%, 14.05%, 20.58%, and 26.47% for RLM, respectively. Regarding M2, the formation rate relative to the other metabolites was 10,06% at 15 min, 10,21% at 30 min, 14,73% at 60 min, and 15,48% at 120 min for HLM, and 13,31%, 13,02%, 19,32%, and 24,81% for RLM, respectively.

For M3, the formation rate relative to the other metabolites was 7.33% at 15 min, 6.80% at 30 min, 7.46% at 60 min, and 9.77% at 120 min for HLM, and 10.25%, 11.73%, 12.89%, and 14.75% for RLM, respectively, and M5 represented less than 5% of the total formation rate. These data indicate that M1 is significantly more abundant in both HLM and RLM, and as its levels decrease over time, the formation rates of M2, M3 and M4 increase. Additionally, M1 shows a higher formation rate in HLM, while the other metabolites exhibit higher formation rates in RLM.

In the phase I + II reaction, the most abundant metabolite in HLM was M7, while in RLM, the formation of M6 and M7 was similar, demonstrating interspecies variation in phase I + II reactions. Considering the phase II reaction, only M7 was formed, with a significantly higher formation rate in HLM, while the area in RLM is approximately 2 % of that observed in HLM.

The differences observed between species may be related to variations in the expression profiles of CYP450 isoforms in humans and animals. These variations include the presence of species-specific isoforms, differences in the relative quantity of each CYP, and variations in enzyme active site binding affinity, resulting in distinct metabolite profiles (Martignoni *et al*., 2006). Figures 8 and 9 present the formation rate of the metabolites over time.

Figure 9. Formation rate of the phase I metabolites over time, considering the total metabolite area *versus* individual areas, using human liver microsomes (HLM) and rat liver microsomes (RLM).

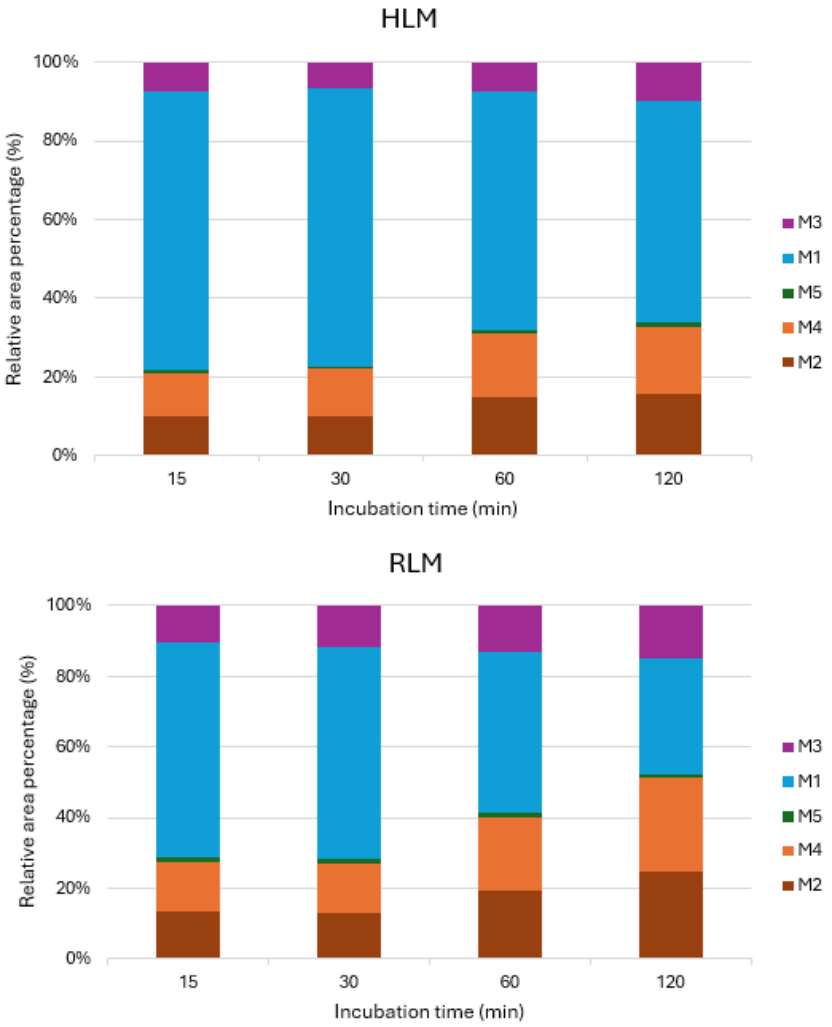

Source. Repository originating from the essay conducted by the authors.

Figure 10. Formation rate of the phase I + II metabolites over time, considering the total metabolite area *versus* individual areas, using human liver microsomes (HLM) and rat liver microsomes (RLM).

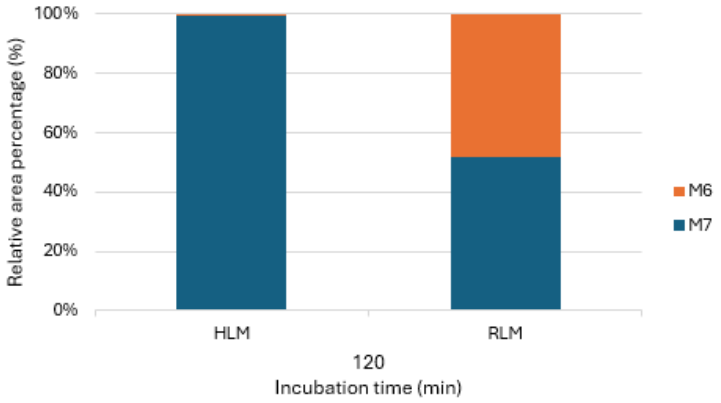

Source. Repository originating from the essay conducted by the authors.

3.4 EVALUATION OF THE INHIBITION OF CYP450 ISOENZYME ACTIVITY USING MONOCLONAL ANTIBODY

After the metabolic identification of dapaconazole and the evaluation of the metabolite formation rate over the incubation period, an *in vitro* enzymatic phenotyping assay was performed using human liver microsomes and monoclonal antibodies, as described in item 2.4. The assay considered all the identified phase I metabolites (M1, M2, M3, M4, and M5). The incubation time was set to 30 minutes, as this period demonstrated a significant formation rate for all metabolites during the identification assay.

After quantification by LC-MS/MS, the ratio between the area of each metabolite and the area of the internal standard was calculated. Subsequently, the percentage of each metabolite formed was related to the negative control (incubation reaction without monoclonal antibody insertion), and the average of the triplicates for each concentration was determined. Table 2 shows the percentage of CYP450 enzyme activity inhibition caused by monoclonal antibodies and the metabolite formation rate relative to the negative control. Figure 10 shows a chart of the percentage of CYP450 enzyme activity caused by monoclonal antibodies for each dapaconazole metabolite identified, in comparison to the negative control. If the antibodies used are highly specific for each CYP450 isoform and cover all isoforms involved in the drug metabolism, the total inhibition caused by these antibodies should approach 100% (Lu *et al.,* 2003).

Table 2. Percentage of CYP450 enzyme activity inhibition caused by monoclonal antibodies for metabolites M1 to M5 and metabolite formation rate relative to the negative control. Data presented as mean ± standard deviation (SD).

Metabolite	M1		M2		M3		M4		M5	
Monoclonal Antibody	Metabolite Formation Rate Relative to the NC (%)	Inhibition (%)	Metabolite Formation Rate Relative to the NC (%)	Inhibition (%)	Metabolite Formation Rate Relative to the NC (%)	Inhibition (%)	Metabolite Formation Rate Relative to the NC (%)	Inhibition (%)	Metabolite Formation Rate Relative to the NC (%)	Inhibition (%)
Anti-CYP1A1	94.4 (2.6)	5.6	86 (4.3)	14.0	99.1 (7.3)	0.9	67.3 (1.4)	32.7	84.9 (12.8)	15.1
Anti-CYP1A2	97.8 (6.3)	2.2	70 (6.6)	30.0	100.7 (4.9)	NA	77.9 (7.6)	22.1	103 (6.1)	NA
Anti-CYP2B6	118.3 (7.4)	NA	82.3 (6.7)	17.7	121 (6.2)	NA	67.8 (1.4)	32.2	119.1 (12.3)	NA
Anti-CYP2C8	86.6 (3.6)	13.4	74.7 (2.7)	25.3	86.2 (4.9)	13.8	63.2 (4.2)	36.8	90.6 (4.6)	9.4
Anti-CYP2C19	87.3 (3.0)	12.7	87 (13.4)	13.0	93 (0.7)	7.0	73.2 (0.7)	26.8	72.2 (9.6)	27.8
Anti-CYP2D6	89.5 (1.8)	10.5	96.5 (4.7)	3.5	91.9 (4.5)	8.1	78.1 (9.0)	21.9	101.7 (5.4)	NA
Anti-CYP2E1	123.9 (8.9)	NA	84.3 (5.1)	15.7	124.3 (0.3)	NA	97 (4.1)	3.0	137.6 (2.6)	NA
Anti-CYP3A4/5	123.6 (4.9)	NA	71 (3.8)	29.0	123.6 (5.2)	NA	115.8 (12.9)	NA	130.8 (3.0)	NA
Sum of the inhibition of all CYPs with a metabolite formation rate relative to the NC < 100%		44.4		148.2		29.8		175.5		52.3

NA: not applicable; NC: negative control
Source. Repository originating from the essay conducted by the authors.

The data demonstrate that the formation of dapaconazole metabolites involves CYP450 isoenzymes, as indicated by the inhibition of metabolite formation rates caused by monoclonal antibodies. Dapaconazole appears to be metabolized by multiple CYP450 isoforms, with overlapping contributions, meaning that more than one isoform may catalyse the formation of the same metabolite. Formation rates exceeding 100% relative to the negative control may suggest saturation of the antibody's binding capacity to its target enzyme, along with compensatory interactions among CYP isoforms. Inhibition of one isoform may lead to increased activity or contributions from others, potentially resulting in unexpected increases in metabolite formation. However, some limitations should be considered when interpreting these findings. Although monoclonal antibodies are designed for high specificity, a certain degree of cross-reactivity is possible, which may affect the accuracy of enzyme attribution. In addition, non-enzymatic factors or spontaneous transformation of intermediates may interfere with metabolite quantification and should not be disregarded.

While these results provide relevant insights into the CYP-mediated metabolism of dapaconazole, further studies using recombinant enzymes and selective chemical inhibitors are necessary to precisely define the individual contribution of each isoform.

Figure 11. Representative chart of the percentage of CYP450 enzyme activity caused by monoclonal antibodies for each dapaconazole metabolite identified, in comparison to the negative control.

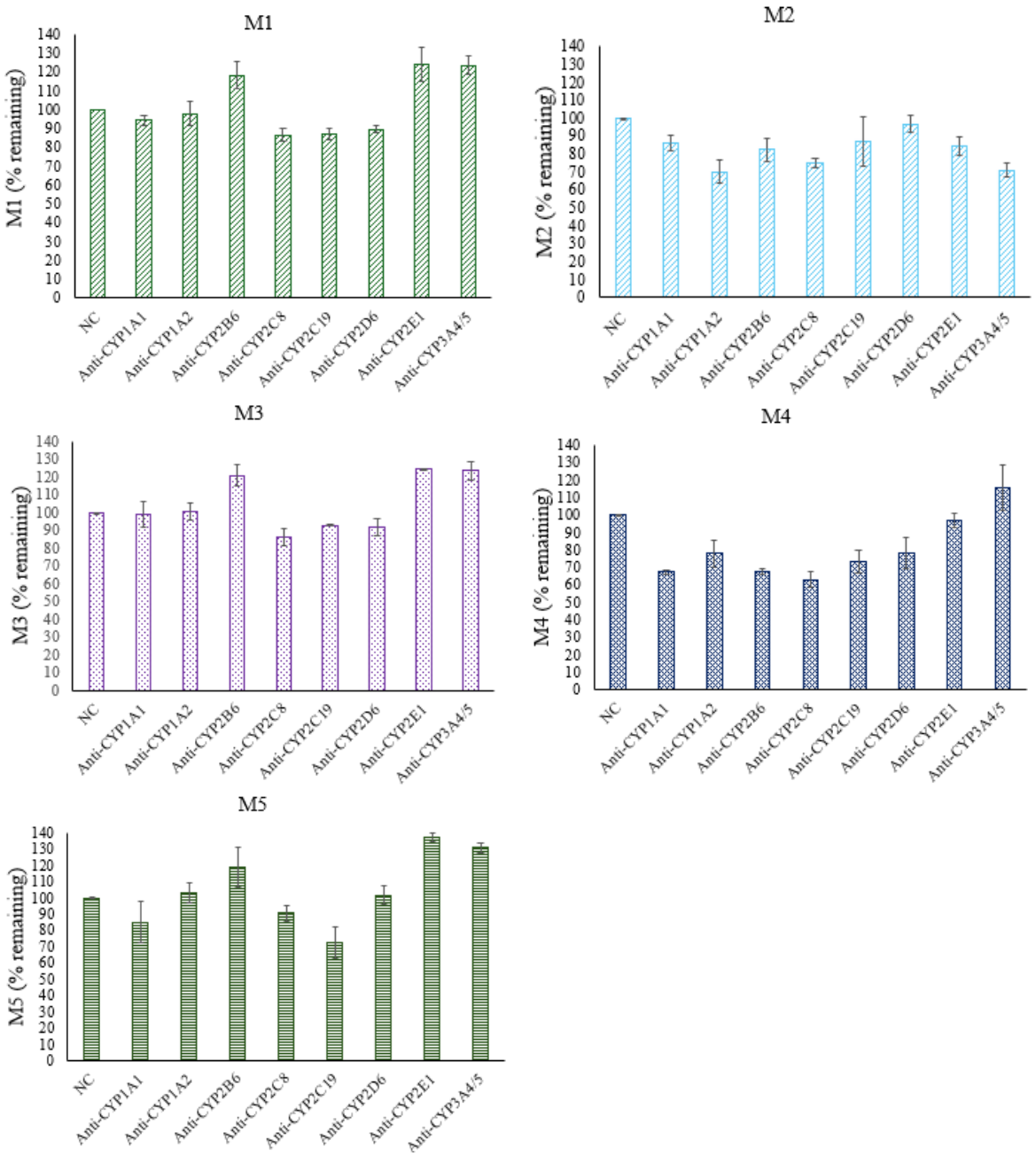

Caption: NC: Negative Control.
Source. Repository originating from the essay conducted by the authors.

4 CONCLUSION

Based on the *in vitro* metabolic identification experiment using HLM and RLM and enzymatic phenotyping assay, five phase I dapaconazole metabolites ($C_{20}H_{18}Cl_2F_3N_2O$, $C_{19}H_{16}Cl_2F_3N_2O_2$, $C_{11}H_{11}Cl_2N_2O$, $C_{19}H_{16}Cl_2F_3N_2O_2$, $C_{19}H_{14}Cl_2F_3N_2O_2$) formed by various isoenzymes of the CYP450 (CYP1A1, CYP1A2, CYP2B6, CYP2C8, CYP2C19, CYP2D6, CYP2E1, CYP3A4), one phase I + II metabolite ($C_{25}H_{24}Cl_2F_3N_2O_8$), and one phase II metabolite($C_{25}H_{24}Cl_2F_3N_2O_7$) were identified. The *in silico* simulation models were valuable for the identification of the metabolites and demonstrated to be an important ally to *in vitro* assays. Herein, we described three new phase I metabolites not reported in the literature and identified, for the first time, dapaconazole conjugated metabolites. Furthermore, the formation profile of these metabolites over time was evaluated. M1 was the most prominent metabolite in both HLM and RLM. Additionally, when analyzing the production of conjugated metabolites, M7 was substantially prominent in HLM when compared to RLM, which produced in equivalent amounts M6 and M7, demonstrating important species variability. The data obtained in this work is important for the next *in vivo* studies of dapaconazole, for which there is potential for systemic administration expansion and new indications, as reported by the company holding the product.

REFERENCES

ALLEN D. *et al.* Azole antifungals: 35 years of invasive fungal infection management. **Expert Rev. Anti Infect. Ther. Early online**, 1–12, 2015.

ANTUNES N. J. *et al. In vitro* metabolism of the new antifungal dapaconazole using liver Microsomes. **Drug Metabolism and Pharmacokinetics**, v. 47, 2022.

ANTUNES N. J. *et al.* Prospective Prediction of Dapaconazole Clinical Drug–Drug Interactions Using an *In vitro to in vivo* extrapolation equation and PBPK modeling. **Pharmaceuticals**, v. 16, n. 28, 2023.

BARREIRO E. J. *et al*. Noções Básicas do Metabolismo de Fármacos. **Química Nova**, v. 19, n. 6, 1996.

BIOLAB WEBSITE, 2022. Available at< https://www.biolabfarma.com.br/imprensa/inovacoes-da-biolab-avancam-no-exterior/>. Accessed on 21-10-24.

BODEY G. P. Azole Antifungal Agents. **Clinical Infectious Diseases**, p. 161-169, v. 14, 1992.

BRADFORD, M.M. A rapid and sensitive method for the quantitation of microgram quantities of protein utilizing the principle of protein-dye binding. **Analytycal Biochemistry**, *v.* 72, 248-254, 1976.

BRUGGEMANN R. J. M. *et al.* Clinical Relevance of the Pharmacokinetic Interactions of Azole Antifungal Drugs with Other Coadministered Agents. **Clinical Infectious Diseases**, v. 48, p.1441–58, 2009.

CANUTO M. M.; RODERO F. G. Antifungal drug resistance to azoles and Polyenes. **THE LANCET Infectious Diseases**, v. 2, 2002.

DE MORAES F. C. *et al*. Quantification of dapaconazole in human plasma using high-performance liquid chromatography coupled to tandem mass spectrometry: Application to a phase I study. **Journal of Chromatography B**, v. 958, p. 102–107, 2014.

DUDDA A.; KUERZEL G. U. Metabolism Studies *in Vitro* and *In Vivo*. **Springer-Verlag Berlin Heidelberg**, 2013.

GAGLIANO-JUCÁ T. *et al*. Phase I Study of the Novel Antifungal Agent Dapaconazole (Zilt®) in Healthy Volunteers. **International Journal of Pharmacology**, v. 10, v. 8, p. 507-512, 2014.

GOBBATO A. A. M. Dapaconazole versus ketoconazole in the treatment of interdigital tinea pedis. Intern. **Journal of Clinical Pharmacology and Therapeutics**, v. 56, n. 1, 2018.

GOBBATO A. A. M. *et al.* A randomized double-blind, non-inferiority Phase II trial, comparing dapaconazole tosylate 2% cream with ketoconazole 2% cream in the treatment of Pityriasis Versicolor. **Expert Opin. Investig. Drugs**, v. 24, n. 11, 2015.

GOBBATO A. A. M. *et al.* Comparison of dapaconazole with miconazole in the treatment of Tinea cruris. **J Eur Acad Dermatol Venereol**, v. 33, p. 54-6, 2019.

GODOI A. B. *et al.* Metabolic Stability and Metabolite Identification of N-Ethyl Pentedrone Using Rat, Mouse and Human Liver Microsomes. **Pharmaceutics**, v.16, n. 2, 2024.

GOMEZ-LECHON M. J. *et al.* Human Hepatocytes in Primary Culture: The Choice to Investigate Drug Metabolism in Man. **Current Drug Metabolism**, 5, 443-462, 2004.

HAVLICKOVA B. e*t al.* Epidemiological trends in skin mycoses worldwide. **Journal compilation Blackwell Publishing Ltd • Mycoses**, v. 51, n. 4, p. 2–15, 2008.

ICH M12 Guideline on drug interaction studies, 2024. Available at https://www.ema.europa.eu/en/documents/scientific-guideline/ich-m12-guideline-drug-interaction-studies-step-5_en.pdf. Accessed on 20-Oct-2024.

JIA L.; LIU X. The Conduct of Drug Metabolism Studies Considered Good Practice (II): *In Vitro* Experiments. **Curr Drug Metab**. 8(8): 822–829, 2007.

LU A. Y. H. *et al.* Cytochrome P450 *in vitro* reaction phenotyping: a re-evaluation of approaches used for p450 isoform identification. **Drug metabolism and disposition**, v. 31, n. 4, 345–350, 2003.

MARTIGNONI M. *et al.* Species differences between mouse, rat, dog, monkey and human CYP-mediated drug metabolism, inhibition and induction. **Expert Opin. Drug Metab. Toxicol**. 2(6), 2006.

NAGAR, S. *et al*. Enzyme Kinetics in Drug Metabolism – Fundamentals and Applications. **Humana Press**, 2014.

NETT, J. E.; ANDES, D. R. Antifungal Agents Spectrum of Activity, Pharmacology, and Clinical Indications. **Infect Dis Clin N Am**, 2016.

NUNES I. K. C. A Importância do Estudo do Metabolismo nos Estágios Iniciais de Desenvolvimento de Fármacos. **Rev. Virtual Quim**., 7 (2), 649-662, 2015.

PALO J. S. *et al*. Pharmacokinetics of Dapaconazole, A Novel Antifungal Agent, in Beagle Dogs and Inhibition of Cytochrome P450 Family 51. **Anti-Infective Agents**, 16, P. 15-21, 2018.

PEARCE R. E. *et al.* Effects of Freezing, Thawing, and Storing Human Liver Microsomes on Cytochrome P450 Activity. **Archives of Biochemistry and Biophysics,** v. 331, n. 2, July 15, p. 145–169, 1996.

PEREIRA D. G. Importância do Metabolismo no Planejamento de Fármacos. **Quim. Nova**, v. 30, n. 1, 171-177, 2007.

WANG F. *et al*. CFM-ID 4.0–a web server for accurate MS-based metabolite identification. **Nucleic Acids Research 50 (W1)**, W165-W174, 2022.

WARRILOW A. G. S. *et al*. Azole Antifungal Sensitivity of Sterol 14α-Demethylase (CYP51) and CYP5218 from Malassezia globosa. **Scientific Reports** | 6:27690, 2016.

YAN Z.; CALDWELL G. W. *In Vitro* Identification of Cytochrome P450 Enzymes Responsible for Drug Metabolism. **Methods in Molecular Biology**, v 1015, 2013.

ZIENTEK M. A.; YOUDIM K. *et al.* Reaction Phenotyping: Advances in the Experimental Strategies Used to Characterize the Contribution of Drug-Metabolizing Enzymes. **Drug Metab Dispos**, v. 43:163–181, 2015.